# Weakly Coupled Proton Interactions in the Malonic Acid Radical: Single Crystal ENDOR Analysis and EPR Simulation at Microwave Saturation

**Einar Sagstuen,*,† Anders Lund,‡ Yoshiteru Itagaki,‡ and Jean Maruani§**

*Department of Physics, University of Oslo, P.O. Box 1048, Blindern, N-0316 Oslo, Norway, Department of Physics and Measurement Techniques, University of Linköping, S-581 83 Linköping, Sweden, and Laboratoire de Chimie Physique, 11 rue de Pierre et Marie Curie, F-75005 Paris, France*

*Received: January 24, 2000; In Final Form: April 17, 2000*

The α-proton hyperfine coupling observed by electron paramagnetic resonance (EPR) spectroscopy on the radical $^{\bullet}CH(COOH)_2$ in irradiated crystals of malonic acid, $CH_2(COOH)_2$, has served as a standard against which hundreds of observations of similar couplings have been held and scaled. The major doublet of the malonic acid radical is accompanied by less intense "forbidden" (f) α-proton transitions and "spin-flip" (s) transitions due to weakly interacting protons. Both s and f transition lines exhibit microwave power saturation behaviors different from that of the major doublet. At high microwave power, the prominence of these s and f lines may be misinterpreted as originating from different radical species. Computer simulations could help distinguish between the different cases, but no computer simulation programs taking into account the microwave power saturation case are commonly available. On the basis of classical line-shape theory, an algorithm describing the microwave power dependence of an EPR line shape has been developed and implemented in an existing simulation program. To test this new program, malonic acid was selected because of the simplicity of its EPR spectra. However, sufficiently detailed information about the hyperfine coupling parameters for a satisfactory simulation of the room-temperature data (including s and f lines) was not available in the literature. Therefore, a detailed room-temperature EPR/ENDOR study on a single crystal of malonic acid was performed. In addition to the major α-proton coupling, seven weaker proton interactions have been characterized and partly identified. Simulations under nonsaturating conditions reproduce very well all features of the experimental EPR spectra. Simulations under saturating conditions similarly reproduce the power-dependent EPR spectra and yield information about the relaxation behavior of the radical system, which is amenable to verification using other spin-resonance methods.

## 1. Introduction

The α-proton hyperfine coupling (hfc) observed in the electron paramagnetic resonance (EPR) spectra of the radical $^{\bullet}CH(COOH)_2$ formed in irradiated crystals of malonic acid, $CH_2(COOH)_2$, has, for four decades, served as the standard against which numerous observations of similar couplings have been held and scaled.[1] McConnell and co-workers[2] used this single proton hfc to experimentally establish the sign of the α-proton coupling, verify the magnitude of the factor relating this coupling to the spin-density population on the neighboring carbon atom,[3] confirm the predicted anisotropy for this type of coupling,[4] and, not the least, discuss the presence and origin of the so-called forbidden transitions. These are represented by resonance lines that, at X-band frequencies, are of smaller intensity, appearing between the two major resonance lines. For illustration, Figure 1a shows a typical (nonsaturated) α-proton EPR spectrum, in which the main lines are designated with (m), the "forbidden" transitions by (f), and the "spin-flip" satellites discussed below as (s). The origin of these extra lines was elucidated at the same time by Miyagawa and Gordy.[5] Both groups made it clear that these lines result from the interplay between the proton Zeeman and hyperfine interactions, which, in general, allows for four EPR transitions.

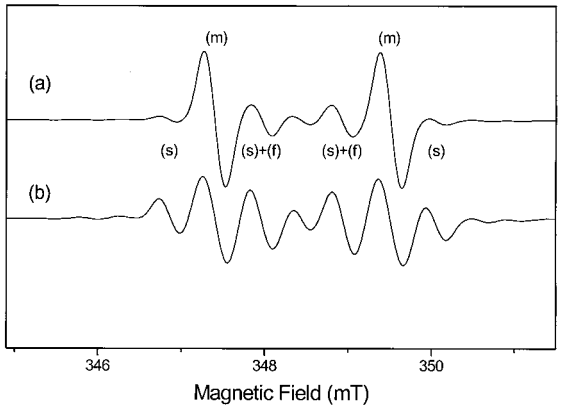


**Figure 1.** First-derivative EPR spectra from an X-irradiated single crystal of malonic acid recorded at 295 K at (a) low and (b) high microwave power. The spectra were recorded using 6.25-kHz modulation at 0.1-mT modulation width. The orientation of the magnetic field is 25.5° from the reference zero point in the rot⟨**a**⟩ plane, corresponding to polar angles $\theta = 49.9°$ and $\varphi = -39.8°$. Spectrum (a) was recorded at 0.2 mW, whereas spectrum (b) was recorded at 100 mW. The two spectra are not in correct relative scales. The various resonance lines have been designated according to their categorization as main lines (m), forbidden transitions (f), and satellite lines (s).

In the years that followed, several papers appeared on the solid-state radiation physics and chemistry of malonic acid. McCalley and Kwiram[6] published a review article on some of this research work and presented a study of malonic acid crystals

* Author to whom all correspondence should be addressed. E-mail: einarsa@fys.uio.no. Telephone: +47 228 55653. Fax: +47 228 55671.
† University of Oslo.
‡ University of Linköping.
§ Laboratoire de Chimie Physique.

10.1021/jp000282p CCC: $19.00 
Published on Web 06/17/2000

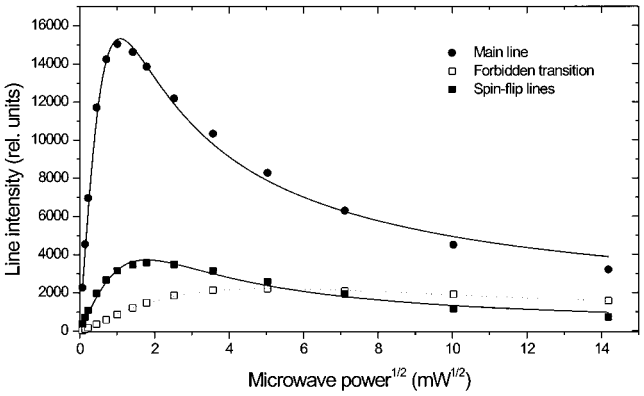


**Figure 2.** Microwave saturation curves for the main lines, forbidden transition lines, and spin-flip lines from a malonic acid single crystal at the same orientation as that shown in Figure 1. As also shown in Figure 1, the two latter lines [(f) and (s)] overlap. This has been corrected for in this figure. Fully drawn curves are the result of fitting experimental data to eq 1. The modulation frequency was 6.25 kHz, with a modulation width of 0.1 mT (p−p).

that were X irradiated at 295 K and studied by electron−nuclear double resonance (ENDOR) spectroscopy at 4.2 K. The authors were able to show that the room-temperature doublet resonance, in fact, represents a thermal average of two conformations of the radical, and they presented detailed parameters for both conformations at 4.2 K. Model calculations showed that these parameters fit McConnell et al.'s[2] room-temperature EPR data very well.

Another spectral feature generally appearing in EPR spectra is the presence of weak satellites on each side of the main lines, separated from them by $\pm g_p\beta_N B$, where $g_p$ is the nuclear *g*-factor for protons (5.585), $\beta_N$ is the nuclear magneton and *B* the magnetic field strength. At X-band frequencies, about 10 GHz, this represents about 0.54 mT, or 15 MHz. Trammell and coworkers,[7] as well as many others,[8] have characterized these satellites as being due to extra protons sufficiently distant from the unpaired electron to give negligible contact hfc, but sufficiently close to it to yield an appreciable dipolar hfc. In proton ENDOR, these interactions give rise to a multitude of resonance lines close to the free proton resonance at $g_p\beta_N B$.

Many computer programs available today[9] are capable of simulating the line shape of a nonsaturated EPR spectrum due to anisotropic couplings, including the forbidden transitions and the spin-flip satellites, provided that the hyperfine interactions are known. However, whereas obtaining the hfc tensors generally is an easy task for the strong interactions, mapping weak interactions requires more advanced techniques, such as ENDOR, and implies a tedious untangling of a complex pattern of lines close to the free proton position.

A further complication may arise. Several workers have shown[10−12] that the forbidden transitions and the spin-flip satellites behave differently from the main lines upon microwave power variation. In general, these resonance lines (called *f* and *s* in Figure 1) saturate more slowly, therefore, appearing more pronounced at high microwave power levels. A typical saturated EPR spectrum for the malonic acid radical is shown in Figure 1b. The detailed power-saturation behavior of the various resonances is illustrated in Figure 2, where the saturation curves for the main lines, forbidden transitions, and spin-flip satellites are shown.

The appearance of relatively intense additional resonance lines at high microwave power levels has often been misinterpreted as being due to other radicals exhibiting different saturation behaviors. In discriminating between the different possibilities, computer simulations would be an easy (and inexpensive) tool to use (using variable microwave frequencies may give clear-cut experimental evidence but is more expensive). However, to our knowledge, no commonly available EPR line shape simulation program takes microwave power saturation effects into account.

In a previous paper,[13] an attempt was made to develop such a program, which included microwave power saturation effects in an empirical manner. This program was successfully applied to the reproduction of the saturation effects observed on the stable radical formed in X-irradiated alanine, an amino acid of considerable importance in the field of EPR dosimetry.[14] The most crucial part of the algorithm was the line shape calculation, in which the main lines were described by the phenomenological equation

$$S(B,P) = K_1\sqrt{P}\sum_{k=1}^{L}\frac{\beta_k g(B - B_k)}{(1 + P/P_0)^{\alpha}} \qquad (1)$$

while the forbidden and spin-flip satellites were assumed to follow a similar relation with the denominator changed to

$$(1 + \beta_k P/P_0)^{\alpha} \qquad (2)$$

Here, *P* is the microwave power, *B* the magnetic field strength, and $B_k$ the field position of resonance line *k*. The exponent $\alpha$ characterizes the shape of the line, such that $\alpha = 1$ for a homogeneously broadened line and $\alpha = {}^1/_2$ for an inhomogeneously broadened line. In this first attempt, several factors were left for trial and error. The distinction (characterized by $\beta_k$) between a main line and a forbidden or spin-flip satellite was empirically chosen. Furthermore, although the parameters $K_1$, $P_0$, $\beta_k$, and $\alpha$ have a clear formal interpretation[13] based on the characteristics of saturation curves, the simplifications of the model required that these parameters also had to be adjusted for optimal fitting to the experimental spectra. This unsatisfactory situation has led us to formulate a physically more stringent algorithm, which was to be incorporated into a general simulation program. Malonic acid was selected as the trial substance to test this new algorithm, because of the simplicity of its radical EPR spectra. However, as the sufficiently detailed information about the radical hyperfine couplings necessary for a satisfactory simulation of the room-temperature spectra was not available in the literature, a detailed EPR/ENDOR study of irradiated malonic acid crystals at this temperature was performed. In the following, an account of these experiments and their interpretation is provided.

## 2. Experimental Procedures

Polycrystalline malonic acid was obtained from Sigma Chemical Co. and used without further purification. Single crystals were grown from saturated aqueous solutions or from solutions in 99.9% $D_2O$ (Sigma Chemical Co.) by slow evaporation at room temperature. The crystals exhibit a characteristic morphology usually similar to that described by McCalley and Kwiram.[6] Malonic acid crystals are triclinic[15] with space group $P\bar{1}$. The crystals used were examined using X-ray diffraction methods and the cell parameters agreed well with the published data.[15] (See Scheme 1.)

Irradiation of the crystals was performed at 280 K using 60-kV, 40-mA X-rays. To eliminate other radicals present in the crystal immediately after irradiation,[2] the crystals were kept in an oven at 340 K for about 15 h after irradiation. Again using X-ray diffraction, the axis of rotation to be used for the EPR/

**SCHEME 1**

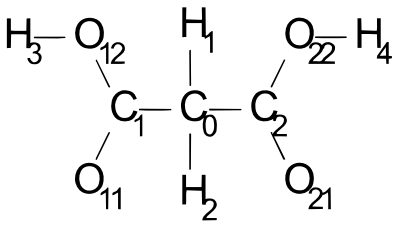


**Malonic Acid**

ENDOR experiments was aligned parallel with one of the crystal axes **a**, **b**, or **c** to within 0.5°. The crystal was then transferred to a quartz rod without loss of alignment. The quartz rod is part of a one-axis goniometer allowing for rotation of the sample through 360° to an accuracy of 0.1°.

The direct crystal axes were used for the actual crystal rotations and measurements. The hyperfine coupling tensor is referred to the orthogonal axis system **a***, **b**′, and **c**. In terms of unit vectors, $\mathbf{a}^* = \mathbf{b} \times \mathbf{c}$, and $\mathbf{b}' = \mathbf{c} \times \mathbf{a}^*$. Simple trigonometry shows that, in this reference system, the rotation axes can be specified in terms of the polar angles $\theta$ and $\phi$ as follows: for **c**, $\theta = 0$, $\phi = 0$; for **b**, $\theta = 102.7°$, $\phi = 90°$; and for **a**, $\theta = 135.17°$, $\phi = -5.95°$.

The spectrometers used for the room-temperature measurements were the Bruker Elexsys 580 system operated in cw mode (Linköping) and the Bruker ESP 300E system, (Oslo) both equipped with the standard Bruker cavities. The rectangular ER4102ST cavity ($TE_{102}$) was used for EPR saturation experiments (modulation frequency 6.25 kHz, modulation width 0.1 mT, and Q $\approx$ 2500) and the Bruker ENDOR cavity ($TM_{110}$) for ENDOR measurements. For the ENDOR experiments, both systems employed Bruker's DICE technology for generation of the rf field. The systems were set to generate a rf-field square-wave-like frequency modulation of the rf field at 12.5 kHz with a modulation depth of typically 100 kHz.

EPR and ENDOR measurements were made by rotating the sample through 5° intervals over 180°. Field splittings and ENDOR frequencies were measured directly on the data acquisition computer screen and fed to the data analysis programs. The program MAGRES[16] was used to derive the hfc tensors from the ENDOR data. A six-parameter linear regression routine generates these tensors from the polar angles of the rotation axes, the measurement angle, and the measured ENDOR frequency. Refinements including a total of nine angles ($\theta$, $\phi$, and the starting angle for each plane) were made, using a nonlinear refinement procedure converging to minimum root-mean-square (rms) value for the complete data set. Providing conservative estimates for the measurement uncertainties, an error analysis was made using the method of propagation of errors,[16,17] yielding standard errors to the principal values of the hfc tensors and to the components of the corresponding eigenvectors. The rms value for the fitting of the major α-proton coupling was 23 kHz, whereas for the weaker proton couplings, the rms values ranged from 12 to 27 kHz. The refined values of the measurement angles obtained from the fitting of the major α-proton coupling were used throughout the analysis for the other couplings. Second-order corrections were not considered.

The crystallographic data program ORFEE[18] was used in conjunction with the reported neutron diffraction atomic parameters[6] to generate inter- and intramolecular atomic contacts and their direction vectors in the ⟨**a***, **b**′, **c**⟩ reference system, yielding results in excellent agreement with those tabulated by McCalley and Kwiram.[6]

Density functional theory (DFT) calculations were performed using the Gaussian 98 program package[19] running on the Cray computer at IFM, University of Linköping. For the isolated malonic acid molecule and the radical, geometry optimizations were done using the B3LYP method and the Pople 6-31G basis set, i.e., the B3LYP/6-31G protocol was used for all calculations. In addition, a chain of three molecules was considered, of which the middle was the malonic acid radical, hydrogen-bonded at each side to undamaged malonic acid molecules. From the initial crystallographic coordinates, the uhf/6-31G protocol was used for an initial geometry optimization to create input coordinates for the subsequent DFT optimizations. As discussed below, the geometry of the undamaged malonic acid molecules was kept fixed, whereas the radical was geometrically optimized without any restrictions. This optimization was further refined using the B3LYP hybrid functional and the 6-31G basis, which also was used for the final single-point calculation.

### 3. Theory of Spectrum Simulation at Microwave Saturation

The influence of microwave power saturation on the shape of inhomogeneously broadened lines has been investigated in various model cases.[10,20,21] To our knowledge however, this influence has not been included in the simulation of EPR spectra except for the analysis of the microwave power dependence of the spin-flip satellites in the spectra of X-irradiated *l*-alanine,[13] where a phenomenological adaptation of the theory of inhomogeneous broadening was attempted. There, except for the saturation factors in eqs 1 and 2, the shapes of the lines were assumed to be identical to that of the unsaturated line. The line shape equations were incorporated in a previously described EPR simulation program.[22]

However, the assumption that the line shape function $g$ is unaffected by saturation is not consistent. According to previous treatments,[10,20,21] one has

$$g(r) \propto \frac{B_k \beta_k}{\Delta B_G} \int_{-\infty}^{\infty} \frac{\exp(-a^2 r'^2)\, dr'}{t^2 + (r - r')^2} \tag{3}$$

where $B_k$ is the resonance field at the maximum of the Gaussian envelope of the Lorentzian spin packets, $\beta_k$ is the transition probability of the line centered at $B_k$, and

$$r = (B - B_k)/\Delta B_L,\ r' = (B' - B_k)/\Delta B_L,\quad a = \Delta B_L/\Delta B_G, \text{ and } t^2 = 1 + s^2 \tag{4}$$

with

$$s^2 = \gamma^2 {B_1}^2 \beta_k T_1 T_2 \tag{5}$$

Here, $\Delta B_L$ and $\Delta B_G$ are related to the full widths at half-height $\lambda'$ and the between points of extremal slopes $\lambda$ of the unsaturated Lorentzian and Gaussian shapes, respectively, by the expressions

$$\Delta B_L = \lambda'_L/2 = \lambda_L\sqrt{3}/2,\ \Delta B_G = \lambda'_G/2\sqrt{\ln 2} = \lambda_G/\sqrt{2} \tag{6}$$

$B$ ($B'$) is the running magnetic field, $\gamma$ the magnetogyric ratio, $B_1$ the strength of the microwave field, and $T_1$ and $T_2$ the spin−lattice and spin−spin relaxation times, respectively, with the assumptions that $T_1 > T_2$ and $T_2 \approx 1/(\gamma \Delta B_L)$. Equation 3 is an adaptation of eq 17 of ref 10 to field-swept EPR in the strong-field approximation.[10] Formally, it is a convolution of a Gaussian, $G_b$, of width $b = 1/a = \Delta B_G/\Delta B_L$, and a Lorentzian, $L_t$, of width $t = \Delta B_L/\Delta B_L = 1$. The assumed independent saturation of spin packets (absence of spectral diffusion) appears in the occurrence of a saturation term in $t$ but not in $b$.

It has been shown[10] that the absorption line given by eq 3, and its corresponding dispersion line, can be cast into the condensed (nonnormalized) form

$$g(r) = (Ds/t)\, u(ar, at),\ h(r) = -(Ds/t)\, v(ar, at)$$

where the Voigt profile $u$ and its Hilbert transform $v$ are the real and imaginary parts, respectively, of the complex error function $w$

$$w(z) = \exp(-z^2)\ \mathrm{erfc}(-\mathrm{i}z)\ (w = u + \mathrm{i}v,\ z = at + \mathrm{i}ar)$$

and $Ds$ depends on the transition probability $\beta_k$ and on the microwave field strength $B_1$.

$$Ds \propto (B_k/\Delta B_L \Delta B_G)\beta_k B_1$$

Substituting the experimentally measured microwave power $P = CB_1^2$ and introducing the spin-relaxation-dependent parameter $P_o = C/\gamma^2 T_1 T_2$ (where $C$ is a proportionality constant that depends on the instrument) in the above expressions for $Ds$ and $t$, one obtains the saturated absorption line shape

$$g(r) \propto (\sqrt{P}/t)\beta_k u(ar, at) \quad (7)$$

$$t = \sqrt{1 + \beta_k P/P_o} \quad (8)$$

In contrast to the phenomenological eq 1, this shape function differs for lines with different degrees of saturation $P$. The saturation factor $t$ also accounts for the difference in saturation behavior between lines with different transition probabilities $\beta_k$. These transition probabilities and the line positions $B_k$ can be computed analytically or numerically, as described in previous papers.[23−25] The standard method[10] consists of analyzing the shapes of unsaturated lines to obtain the Lorentzian and Gaussian widths, $\Delta B_L$ and $\Delta B_G$, and then the saturation curves, to yield $P_o$, from which the relaxation times can be derived. In this paper, the homogeneous and inhomogeneous broadenings were estimated by a comparison between experimental and simulated line shapes, $P$ was obtained from the spectrometer settings, and $P_o$ was estimated by fitting a series of power-dependent experimental line shapes. The overall absorption line shape can be written as a sum of absorption components, as given by eq 7 (where the dependence of both the shape function $u$ and the saturation factor $t$ on the transition probability $\beta_k$ is stressed by the label $k$).

$$S(B,P) \propto \sqrt{P} \sum_{k=1}^{L} \beta_k\, u_k(ar, at)/t_k \quad (9)$$

Experimentally, the first derivatives of the absorption spectra were recorded, and therefore, we used as a parameter the peak-to-peak width (i.e., the width between points of extremal slopes in the absorption line shape). The relevant normalized component derivatives are then written as

$$g'(x) \propto -\{P/(1 + \beta_k P/P_0)\}^{1/2} \beta_k\, u'(xa\rho_{a,t}, at)/u'(\lambda a\rho_{a,t}, at) \quad (10)$$

where $u'$ is the derivative of the nonnormalized Voigt profile $u$ and $\lambda$ is half of the measured peak-to-peak width, $x$ is the running field variable, $a$ is the convolution parameter defined in eq 4, and $a\rho_{a,t}$ is the abcissa of the maximum of $u'$ for given $a$ and $t$.

The above formulas were incorporated in computer programs developed previously for the calculation of crystal and powder EPR line shapes under nonsaturating conditions.[22] It should be noted that, in the present paper, however, the calculated absorption spectra were numerically normalized and differentiated, and eq 10 was hence not used explicitly.

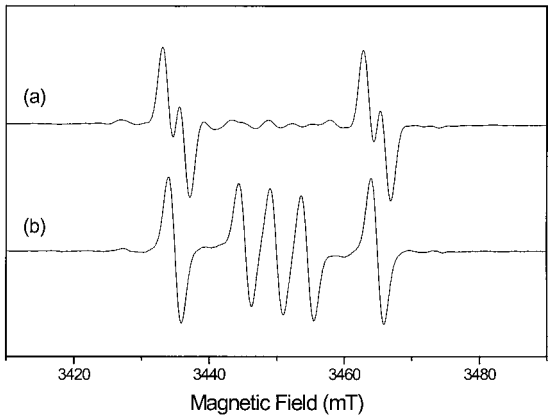


**Figure 3.** First-derivative EPR spectra from X-irradiated (a) normal and (b) partially deuterated single crystals of malonic acid at the same orientation of the magnetic field, which is 31.8° from the reference zero point in the rot⟨**b**⟩ plane, corresponding to polar angles $\theta = 143.5°$ and $\varphi = 28.2°$. The central triplet in (b) is due to the major radical with the α-proton exchanged with a deuteron.

## 4. Experimental Results and Analyses

EPR spectra from the $^{\bullet}CH(COOH)_2$ radical in irradiated malonic acid crystals are well-known in the literature,[2,6] and a typical example is given in Figure 1a. However, it should be mentioned that additional splitting of the main lines occurred at some orientations (Figure 3a). This additional splitting vanished in the partially deuterated crystals (Figure 3b), indicating that it is due to a weak interaction with an easily exchangeable proton. Previous authors[26] have made similar observations, but without data from deuterated crystals, they suggested that this splitting is due to two conformations of the radical at room temperature.

It should also be mentioned that, when partially deuterated crystals are used, an intense triplet appears in the middle of the EPR spectrum (Figure 3b). The analysis shows that it is due to the radical $^{\bullet}CD(COOD)_2$, indicating that partial deuteration of the methylene protons also takes place when malonic acid is dissolved in $D_2O$, even at room temperature. A detailed ENDOR analysis of the deuterium hyperfine and quadrupolar couplings will be reported elsewhere.[27]

Figure 4 shows a typical ENDOR spectrum in the range 10−50 MHz, together with the respective (second derivative) EPR spectrum and also the ENDOR-induced EPR (EIE) spectra. ENDOR lines have been labeled according to the designations of the hfc tensors given in Table 1. In the high-frequency region, the spectrum is dominated by the $\nu^+$ branch of the major α-proton coupling, and this line was used to evaluate the corresponding hfc tensor. (Note that, in this paper, an ENDOR line is superscripted with + if it belongs to the $M_s = {}^1/_2$ manifold of states and with − if it belongs to the $M_s = -{}^1/_2$ manifold.)

Figure 5 shows the angular variation plot for this resonance line for rotation about ⟨**b**⟩. Data from the corresponding rotation plane for a partially deuterated crystal are included in this figure, but have not been used in the fitting procedure. The derived hfc tensor is given in Table 1. In addition, some very weak lines due to (an)other radical species remaining after thermal annealing are apparent in Figure 4. An instrumental artifact appears at the ${}^1/_2\nu_\alpha^+$ frequency, because of the second harmonic component of the rf field generated by the amplifier.

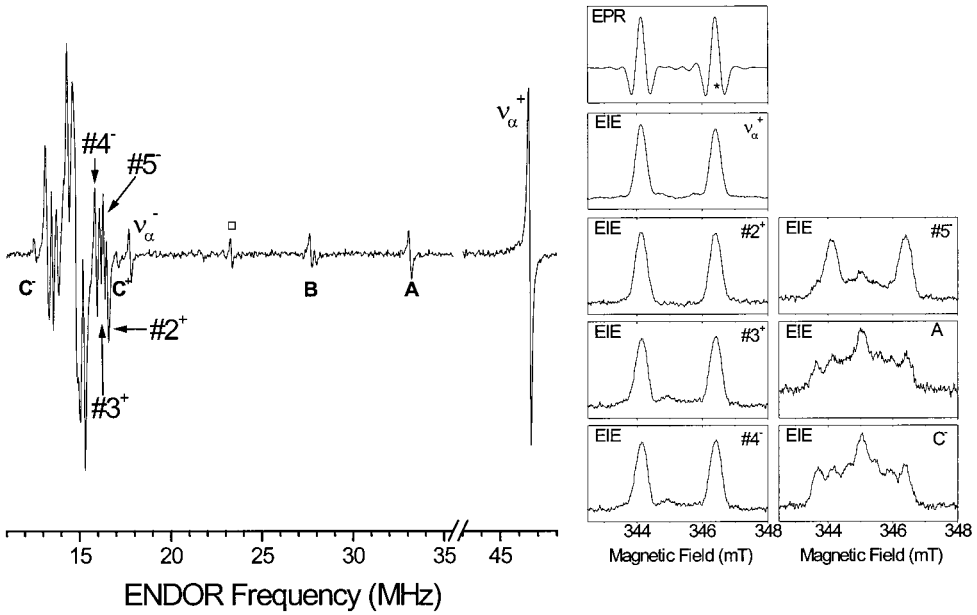


**Figure 4.** ENDOR spectrum from an X-irradiated single crystal of malonic acid at 295 K. The orientation of the magnetic field is 66.8° from the reference zero point in the rot⟨**b**⟩ plane. The insets show the corresponding second-derivative EPR (top) spectrum and EIE spectra, recorded off the indicated resonance positions of the ENDOR spectrum. Resonance line designations correspond to the hyperfine coupling tensor designations in Table 1, except for lines A, B, and C, which are due to (an)other radical species. The line marked by a square is an instrumental artifact. The ENDOR spectrum was recorded at a magnetic field value marked by * in the top inset figure.

**TABLE 1: Hyperfine Coupling Parameters for the Major Radical in Malonic Acid, X Irradiated and Observed by ENDOR at 295 K**[a]

| tensor | principal values (MHz) | isotropic value (MHz) | dipolar coupling (MHz) | eigenvectors ⟨**a***⟩ | ⟨**b′**⟩ | ⟨**c**⟩ |
|---|---|---|---|---|---|---|
| | −90.25 (7) | | −32.19 | 0.0406 (24) | 0.4074 (1) | 0.9124 (2) |
| $\nu_\alpha^+$ | −56.52 (1) | −58.06 (4) | 1.54 | 0.9991 (1) | −0.0513 (6) | −0.0423 (6) |
| | −27.42 (3) | | 30.64 | −0.0128 (8) | 0.9133 (2) | −0.4072 (1) |
| | 3.57 (5) | | 5.27 | −0.0602 (40) | 0.0585 (102) | 0.9964 (3) |
| **2** | −4.15 (1) | −1.70 (3) | −2.45 | 0.9910 (17) | 0.1230 (98) | 0.0526 (38) |
| | −4.53(1) | | −2.83 | 0.1195 (186) | −0.9907 (21) | 0.0653 (73) |
| | 4.14 (5) | | 4.76 | 0.0796 (45) | 0.2117 (49) | −0.9741 (5) |
| **3** | −2.69 (1) | −0.62 (3) | −2.07 | 0.7720 (111) | −0.6313 (110) | −0.0741 (44) |
| | −3.32 (1) | | −2.70 | 0.6306 (62) | 0.7461 (76) | 0.2137 (26) |
| | 3.53 (2) | | 3.42 | 0.9740 (26) | 0.1445 (38) | −0.1743 (92) |
| **4** | −1.45 (2) | 0.11 (1) | −1.56 | 0.1386 (288) | 0.2280 (1521) | 0.9638 (289) |
| | −1.76 (1) | | −1.87 | 0.1790 (166) | −0.9629 (323) | 0.2020 (353) |
| | 3.20 (2) | | 3.22 | 0.9549 (24) | 0.0838 (102) | 0.2849 (43) |
| **5** | −0.29 (10) | −0.02 (10) | −0.27 | 0.2201 (103) | −0.8438 (60) | −0.4895 (74) |
| | −2.96 (14) | | −2.94 | 0.1994 (56) | 0.5301 (96) | −0.8242 (40) |
| | 5.87 (6) | | 3.58 | 0.0793 (137) | 0.8129 (49) | 0.5770 (35) |
| **6** | 0.68 (10) | 2.29 (15) | −1.61 | 0.5431 (1966) | 0.4501 (977) | −0.7088 (1193) |
| | 0.31 (24) | | −1.94 | −0.8359 (473) | 0.3696 (1137) | −0.4058 (1763) |
| | 5.18 (27) | | 5.03 | −0.0672 (123) | −0.5802 (56) | 0.8117 (35) |
| **7** | −1.03 (3) | 0.15 (16) | 0.88 | 0.9822 (15) | 0.1047 (111) | 0.1562 (74) |
| | −3.69 (7) | | −3.83 | 0.1757 (78) | −0.8077 (34) | −0.5628 (33) |
| | 9.66 (2) | | 4.18 | 0.4197 (18) | 0.7730 (22) | 0.4758(34) |
| **8**[b] | 3.61 (2) | 5.48 (3) | −1.87 | 0.3526 (348) | −0.6219 (80) | 0.6992 (62) |
| | 3.18 (3) | | −2.30 | 0.8364 (229) | −0.1257(480) | −0.5335 (422) |

[a] Numbers in parentheses are uncertainties in the last significant digit(s) of the corresponding number. [b] Measured at 242 K (−31 °C), see text.

The 10−20 MHz part of the ENDOR spectrum in Figure 4 shows a number of resonance lines. From the detailed analysis of the three planes of rotation, it turns out that six of these lines exhibit sufficient anisotropic behavior to contribute to the observed spin-flip lines. Each of the lines was examined using the EIE technique and ascertained to be associated with the main radical species. Figure 5 shows the angular variation plot for the six lines for rotation about ⟨**b**⟩, together with the theoretically predicted variations based on the hfc tensors given in Table 1.

As mentioned above, an extra doublet was observed at several orientations of the crystal in the magnetic field (Figure 3a). This doublet was not apparent in partially deuterated crystals, suggesting that it is due to an interaction with an easily exchangeable proton. Surprisingly, however, the ENDOR

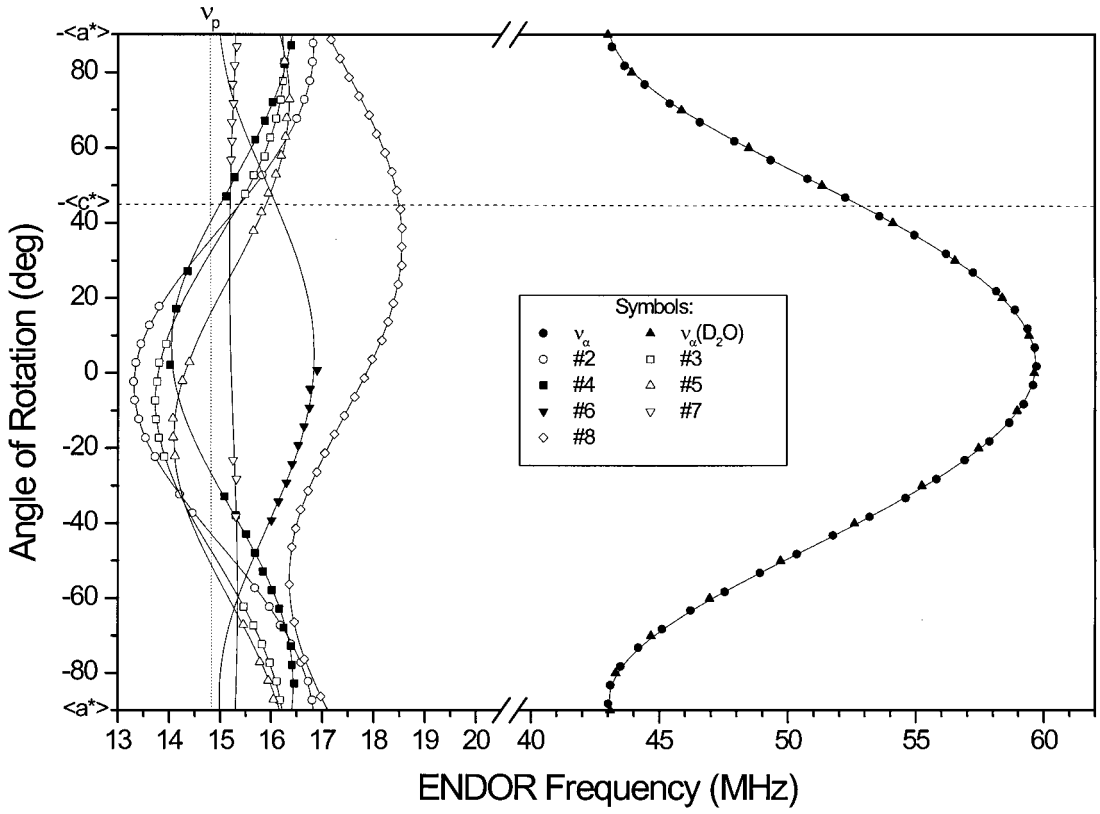


**Figure 5.** Angular variation plot (rotation about ⟨**b**⟩) for the ENDOR lines analyzed in the present work. Symbol explanation is given in the inset. One plane of data for the $\nu_\alpha^-$ line of the α-proton coupling obtained using a partially deuterated crystal has been included in the figure, but these data were not used in the fitting procedure. The fully drawn curves are calculated using the hyperfine coupling parameters given in Table 1.

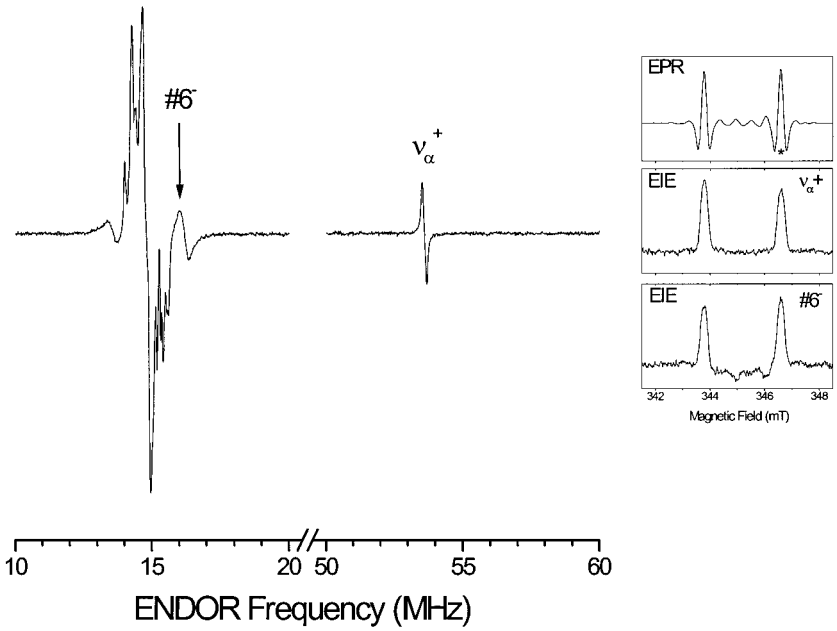


**Figure 6.** ENDOR spectrum from an X-irradiated single crystal of malonic acid at 295 K. The axis of rotation is ⟨**b**⟩, with the magnetic field −38.2° from the reference zero point. The insets show the corresponding second-derivative EPR (top) spectrum and EIE spectra, recorded off the indicated resonance positions of the ENDOR spectrum. Resonance line designations correspond to the hyperfine coupling tensor designations in Table 1. The ENDOR spectrum is recorded at a magnetic field value marked by * in the top inset figure.

spectrum due to this additional resonance could not be observed at room temperature. In addition, at several orientations, the ENDOR line whose analysis yielded the hfc tensor **6** in Table 1 broadened to an extent that made it unobservable over large regions. Figure 6 shows an ENDOR spectrum at an orientation where this line starts broadening; only 15−20° from this orientation the line is no longer observable. The EIE spectra shown in Figure 6, however, unequivocally show that this coupling is associated with the main radical species.

It was speculated that the failure to observe the larger hyperfine coupling giving rise to the observable EPR splitting may be due to a large thermal amplitude of the proton motion, resulting in enhanced nuclear relaxation and corresponding broadening of resonance lines. Experiments were made at lower

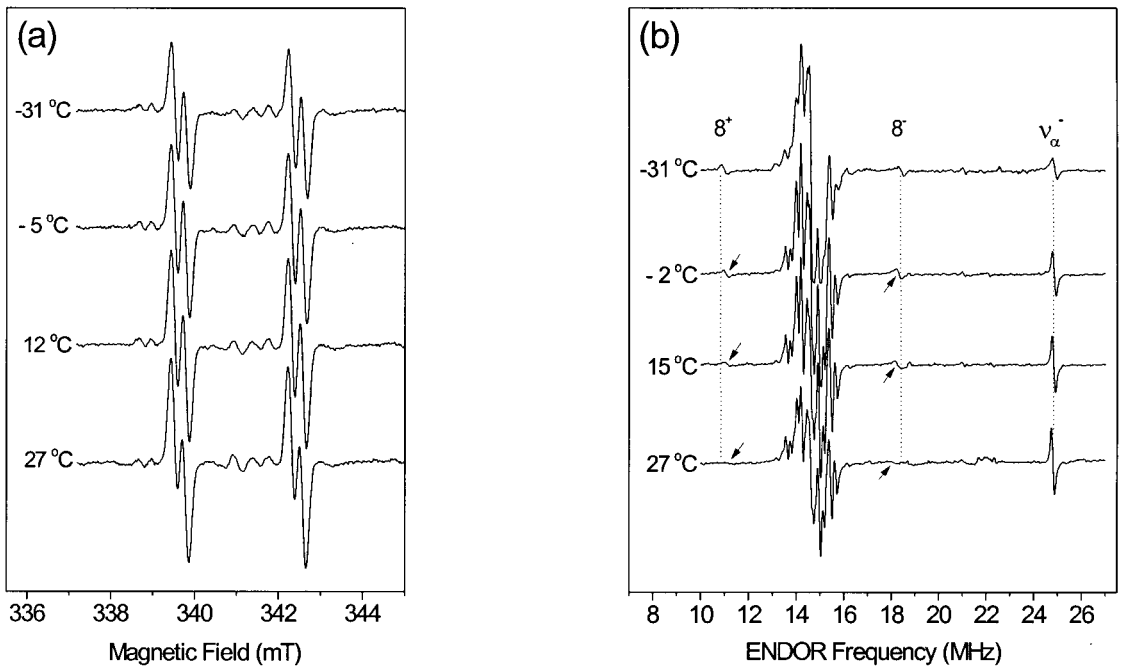


**Figure 7.** Temperature dependence of hyperfine coupling **8** from malonic acid, recorded with the magnetic field 155.8° from the reference zero point in the rot⟨**a**⟩ plane. (a) Temperature variation of the EPR spectra and (b) corresponding data for the ENDOR spectra. The arrows indicate the actual ENDOR line positions of coupling **8**.

temperatures to test this hypothesis and eventually determine the coupling tensor by ENDOR.

At a given orientation of the malonic acid crystal, where the doublet was clearly resolved, the crystal was cooled in steps from room temperature and allowed to temperature stabilize at each step before EPR/ENDOR measurements were made. Figure 7a shows the EPR spectra recorded at some of these temperatures. Apparently, the doublet splitting increases slightly upon cooling (about 0.03 mT at this orientation), as can be seen from the increasing resolution of the small coupling. Figure 7b shows the concomitant changes in the ENDOR spectra during the cooling process. Even around 15 °C, the additional ENDOR lines associated with this extra doublet splitting are clearly visible. The crystals were cooled to about −30 °C, and measurements were made in all three planes of rotation. From these measurements, the hfc tensor denoted **8** in Table 1 was extracted. The ENDOR line angular variation plot for coupling **8** is included in Figure 5. EIE spectra (not shown) were recorded from the corresponding ENDOR lines, confirming that they represent a coupling associated with the main radical species.

Also on the spectra shown in Figure 7b, it can be seen that the frequency of the ENDOR lines of coupling **8** changes with temperature, increasing (decreasing) upon increasing the temperature [about 0.4 MHz for lines $\mathbf{8}^+$ ($\mathbf{8}^-$) at this orientation]. Therefore, to simulate the EPR spectra at room temperature (see below), the value of the maximum principal element of its hfc tensor was reduced by 1.3 MHz. (This corresponds to the 0.4 MHz frequency shift value of ENDOR lines at the orientation shown in Figure 8.) This procedure is rather imprecise but was chosen so as to reach an optimal fit between the simulated and experimental spectra at 300 K.

It is interesting to notice on the spectra shown in Figure 7b that the $\nu_\alpha{}^+$ ENDOR line for the major coupling broadens appreciably (∼40%) between 300 and 242 K, whereas the frequency of the resonance line position barely changes (0.06 MHz). McCalley and Kwiram[6] showed that the room temperature spectra could be explained by thermal averaging of two conformations of the major radical being clearly distinguishable at low temperatures. The observed broadening (Figure 7b) may indicate that the thermal averaging is effective at 300 K, but not at 242 K.

## 5. Simulations

The single-crystal simulations for the malonic acid radical, which involve $4^8 = 65\,536$ transitions due to one major α-proton and seven weakly coupled protons, required computation times of 1−2 min per spectrum using a 200-MHz Pentium system. The experimental spectra could be well reproduced in the microwave power range from 0.005 mW through 200 mW using the parameters $P_o = 0.04$ mW, $\lambda_L = 0.0018$ mT, and $\lambda_G$ as specified below.

**5.1. Unsaturated Spectra.** A series of experimental, low-microwave-power EPR spectra were simulated using the hfc parameters given in Table 1 to determine whether the ENDOR data properly reproduced the EPR spectra. Figure 8 shows simulations performed in the three planes of rotation at orientations where the extra hfc (**8**) exhibits sufficient magnitude for observable resolution. At these orientations, an isotropic line width $\lambda_G = 0.11$ mT was used. As commented above, the value of the maximum principal element of **8** was reduced by 1.3 MHz to account for the reduction in coupling value due to the higher measurement temperature. An excellent agreement is obtained.

**5.2. Microwave Power Dependence.** A few representative microwave power-dependent simulated spectra are shown in Figure 9. At this orientation, the inhomogeneous line width used was $\lambda_G = 0.2$ mT. The finding that $\lambda_G$ is 2 orders of magnitude larger than $\lambda_L$ characterizes inhomogeneous broadening.[21,28] A comparison with the experimental spectra in Figure 9 again shows excellent agreement.

One may notice that the relaxation times $T_1$ and $T_2$ may be the more physically adequate parameters to use in line shape simulations. This, however, would require that the instrument

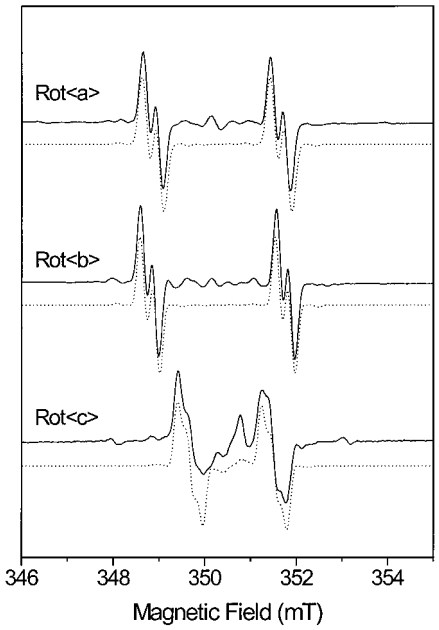


**Figure 8.** Experimental (solid lines) and simulated (dotted lines) EPR spectra from malonic acid at room temperature. The microwave power is 0.5 mW, and the modulation frequency is 6 kHz at a width 0.11 mT. The orientations of the magnetic field are as follows: (a) 150.8° from the reference zero point in the rot⟨**a**⟩ plane, corresponding to polar angles $\theta = 51.5°$ and $\varphi = 33.0°$; (b) same as Figure 3; and (c) 125.6° from the reference zero point in the rot⟨**c**⟩ plane, corresponding to polar angles $\theta = 90.0°$ and $\varphi = -54.4°$.

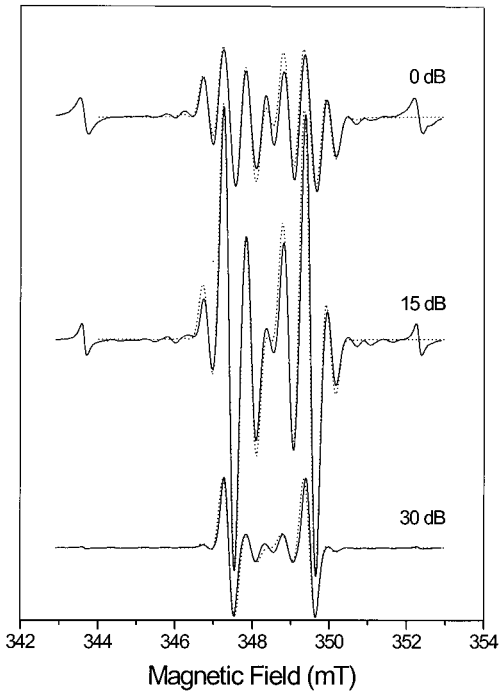


**Figure 9.** First-derivative EPR spectra from an X-irradiated single crystal of malonic acid single crystal at the same orientation as that shown in Figure 1 for different microwave powers. Dotted line spectra are simulations with parameters $P_0 = 0.04$ mW, $\lambda_L = 0.0018$ mT, and $\lambda_G = 0.2$ mT, as defined in the text, and with hyperfine coupling data of Table 1. The outermost resonance lines are due to a $Mn^{2+}$/MgO sample used for reference purposes.

factor $C$ be determined and/or that separate measurements using FT-EPR techniques be made.

For the malonic acid radical, $T_1$ in the crystalline matrix has, in fact, been determined previously[29] to be about 40 $\mu$s. Furthermore, for the standard Bruker EPR cavity (ER 4102ST) the conversion factor $c$ in the relation

$$B_1 = c\sqrt{PQ}$$

was determined to be $1.4 \times 10^{-4}$ T $W^{-1/2}$ at a $Q$-factor of 2500.[29] $T_2$ may then be estimated by two different procedures, based on parameters obtained from fitting to the microwave power-dependent simulations. First, from the relations $T_2 \approx 1/\gamma\Delta B_L$ and $\Delta B_L = \lambda_L\sqrt{3}/2$ with $\lambda_L = 0.0018$ mT, $T_2$ is calculated to 3.6 $\mu$s. Second, from the conversion factor relation above, $P = CB_1^2$ with $C = 1/c^2$. Now, using the relaxation-dependent parameter $P_o = C/\gamma^2 T_1 T_2$ with $P_o = 0.04$ mW and $T_1 = 40$ $\mu$s, $T_2$ is estimated to 1 $\mu$s. The agreement between these two estimates of $T_2$ is reasonable considering the trial-and-error procedure followed to obtain the values for $\lambda_L$ and $P_o$.

## 6. Molecular Orbital Calculations

A series of calculations based on density functional theory as implemented in the Gaussian 98[19] program have been performed to learn more about structural details of the malonic acid radical. In all instances, crystallographic data obtained from neutron and X-ray diffraction measurements[6,15] were used as input parameters.

The conformation of the malonic acid molecule in the native crystal is particular in that the two carboxyl groups are twisted by about 90° with respect to each other. This is illustrated in Figure 10, which shows the content of one unit cell of the malonic acid crystal. One of the carboxyl groups ($-C_1O_{11}O_{12}$) is almost coplanar with the $C_2-C_0-C_1$ backbone, whereas the other exhibits an angle of twist of 89.6°. The major difficulty encountered in the calculations was the inherent, strong tendency for the malonic acid radical to become fully planar. Leaving no constraints on the geometry optimization for an isolated malonic acid radical except for an initial assumption of $sp^2$ hybridization at $C_0$, the twisted carboxyl group ($-C_2O_{21}O_{22}$) rotates and becomes coplanar with the remainder of the radical. It is unreasonable that this will happen in a crystal lattice because of crystal packing constraints, most importantly the relatively firm anchoring of each carboxyl group by hydrogen bonding to neighboring malonic acid molecules. Several ways of approximating a physically more realistic radical structure were tried.

For the most comprehensive of these, a sequence of three molecules (a trimer) was constructed so that the central radical species is hydrogen-bonded to neighboring (undamaged) malonic acid molecules. It was, however, necessary to completely fix the geometry of the two terminating malonic acid molecules to their crystallographic conformations and leave only the radical geometry for optimization. This input configuration is depicted in Figure 11a. Even with these restrictions, the final energy-optimized conformation of the trimer showed that the twisted carboxyl group rotated by about 25° toward a more planar structure. During this process, the $C_2-C_0(H_\alpha)-C_1$ backbone was slightly changed. First, the plane of the backbone forms an angle of about 6° with that of the initial (crystallographic) conformation. Second, the radical $C_0-H_\alpha$ bond direction is rotated by 12.6° from its initial direction. This angle can be decomposed to about 10° out of the initial $C_2-C_0-C_1$ plane and 5.5° from the internal bisector of the initial $C_2-C_0-C_1$ backbone, in the (initial) $C_2-C_0-C_1$ plane. Figure 11b shows the optimized geometry of the trimer radical structure. It is possible that, in the crystal, this kind of reorganization may be further enhanced,

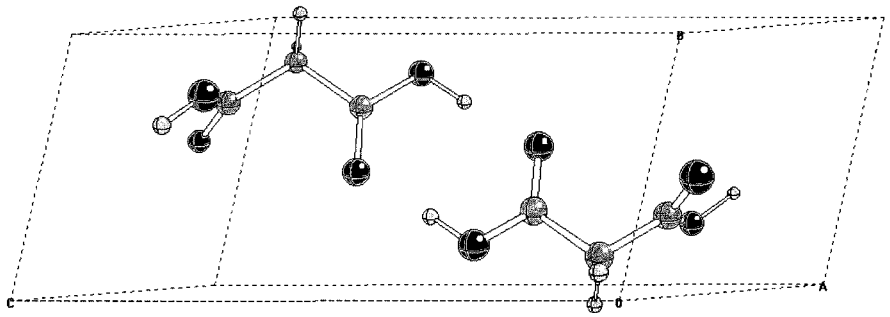


**Figure 10.** The malonic acid crystal unit cell with both asymmetric units included. The larger globes represent oxygen atoms, and H atoms are represented with the smaller spheres.

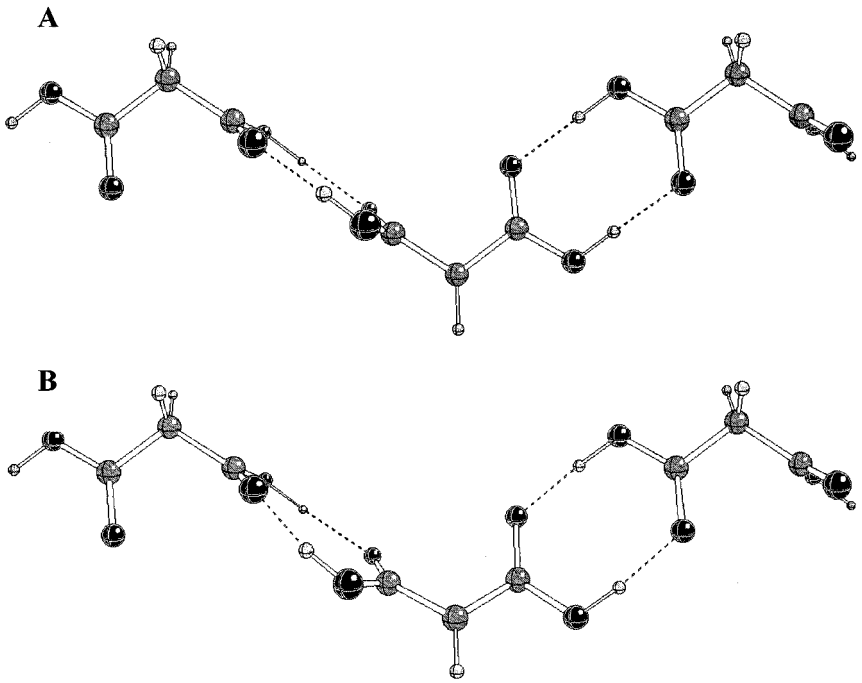


**Figure 11.** The trimer structure of the malonic acid radical complex used for the DFT calculations. (A) Input structure from crystallographic data. (B) Energy-optimized structure.

as also the neighboring malonic acid carboxyl groups may partly relax to a more planar configuration.

It must be emphasized, however, that even this trimer model cannot, in any respect, account for all intermolecular packing constraints of the radical in the molecular crystal. Thus, the results can be taken only as indications of possible actual radical geometries. The major observation is that the $C_0-H_\alpha$ bond may, to some extent, become rotated from its initial crystallographic direction to allow for an enhanced planarity of the entire radical geometry.

Table 2 shows the hyperfine coupling parameters obtained from a single-point calculation of the geometry-optimized trimer radical structure. These results will be discussed further below.

**TABLE 2: Hyperfine Coupling Parameters (in MHz) for the Major Radical in Malonic Acid, Calculated Using DFT Methods and Experimental Values**

| | calculated | | experimental | |
|---|---|---|---|---|
| atom | $a_{iso}$ | $a_{dip}$ | $a_{iso}$ | $a_{dip}$ |
| | | 38.0 | | 30.6 |
| $H_\alpha$ | −66.1 | −5.6 | −58.1 | 1.5 |
| | | −32.4 | | −32.2 |
| | | 5.1 | | 4.2 |
| $H_4$ | 7.4 | −2.9 | 5.5 | −2.3 |
| | | −2.2 | | −1.9 |
| | | 5.7 | | 5.3 |
| $H_3$ | −4.3 | −3.1 | −1.7 | −2.8 |
| | | −2.6 | | −2.5 |
| | | 4.0 | | 4.8 |
| $H_{4'}$ | −0.5 | −2.0 | −0.6 | −2.7 |
| | | −2.0 | | −2.1 |
| | | 6.6 | | 3.6 |
| $H_{3'}$ | −0.4 | −3.6 | 2.3 | −1.9 |
| | | −3.0 | | −1.6 |

## 7. Aspects of Radical Structure

McConnell et al.[2] described the molecular structure of the main radical formed in malonic acid crystals after room-temperature irradiation. According to McCalley and Kwiram,[6] the room-temperature EPR parameters result from thermal averaging of different conformations of the radical, which only become amenable for detailed study upon lowering the temperature.

It appears that the eigenvectors of the room-temperature (RT) α-proton coupling tensor deviate significantly, in some respects, from those expected from the crystallographic data, assuming $sp^2$ hybridization at $C_0$. Thus, the direction of the intermediate principal value is 11.7° from the perpendicular to the crystallographic $C_2-C_0-C_1$ molecular backbone, and the eigenvector for the minimum principal value is 24° from the in-plane bisector

of the $C_2-C_0-C_1$ fragment. Considering the results from the DFT calculations above, however, it is reasonable to assume that these deviations result from molecular reorganization upon radical formation.

It is not the purpose of this paper to give a detailed analysis of the weakly coupled proton interactions. However, a few comments will be made. It is evident that there can be only two further intramolecular proton interactions in the radical, that is, those involving the two hydroxyl protons (Figures 10 and 11). Of the two hydroxyl protons, one ($H_3$) is situated almost exactly in the nodal plane of the radical, being bonded to the $-C_1O_{11}O_{12}$ carboxyl group coplanar with the $C_2-C_0-C_1$ molecular backbone. The other proton ($H_4$) is out of the radical plane, being bonded to the $-C_2O_{21}O_{22}$ carboxyl group twisted about 65° away from the $C_2-C_0-C_1$ molecular backbone. These interactions may both be expected to exhibit significant isotropic contributions to the hyperfine interaction. Couplings **2** and **8** are the most probable candidates for the two intramolecular hydroxyl proton interactions. With $H_3$ being almost in the plane, the $H_3$ coupling (with contributions from spin densities at both $C_0$ and $O_{11}$) is expected to exhibit a maximum principal direction with a negligible $\langle \mathbf{a}^* \rangle$ component and one principal direction along $\langle \mathbf{a}^* \rangle$. Coupling **2** agrees with these considerations and with the hyperfine couplings calculated from the single-point DFT calculation on the energy-optimized trimer structure (Table 2). The $H_4$ coupling with the main component from the $C_0$ spin density only would have a maximum principal direction significantly out of the plane and a more axially symmetric coupling tensor. Coupling **8** is in agreement with this.

In addition, the coplanar carboxyl group has a significant amount of delocalized spin density, mainly located at the aromatic oxygen $O_{11}$. According to INDO-type calculations,[30] this may amount to more than 20%. $O_{11}$ is hydrogen-bonded to a hydroxyl proton ($H_3'$) of a neighboring molecule, and a significant coupling will result. In addition, a smaller contribution from the interaction with the major spin density at $C_0$ (about 0.77)[6] is expected. Coupling **6** is assigned to this interaction. The calculated results for $H_3'$ differ somewhat, however, from the experimental values for coupling **6**. Finally, the proton ($H_4'$) that is hydrogen-bonded to $O_{21}$ is expected to exhibit an out-of-plane hfc tensor, and coupling tensor **3** is assigned to this interaction.

The remaining three couplings are all smaller and, in particular, all exhibit small isotropic values. Considering the chain of reactions leading to the formation of stable radicals in malonic acid,[31] the radical environment is expected to become altered with respect to the pristine crystal structure. It may, however, be mentioned that couplings **4** and **5** have their maximum values directed almost perpendicular to the $C_2-C_0-C_1$ molecular backbone. $H_3''$ and $H_1'$ of two neighboring molecules are located almost directly "over" and "under" $C_0$ of the malonic acid radical. The dipolar couplings of these two interactions indicate interatomic distances of about 3.5 Å, as compared to the $C_0\cdots H_3''$ distance of 3.6 Å and the $C_0\cdots H_1'$ distance of 3.8 Å. Coupling **7** is an in-plane type of interaction but is not easily identifiable from the crystal structure analysis.

**Acknowledgment.** We are indebted to Dr. William H. Nelson for providing the EPR/ENDOR analysis program MAGRES and for his help with the ORFEE calculations and to Dr. Peter Höfer who provided the conversion factor for the Bruker 4102ST rectangular cavity and information on his measurements on the malonic acid radical relaxation times. Helpful discussions with Mr. Audun Sanderud are acknowledged. This work was supported in part of a grant (E.S.) from the Wenner-Gren Stiftelserna, Sweden, and by a network grant from the Nordic Academy for Advanced Research (NorFA). Y.I. and A.L. acknowledge support from the Swedish Foundation for International Cooperation in Research and Higher Education (STINT) and the Swedish Natural Science Research Council.

## References and Notes

(1) Goslar, J.; Piekara-Sady, L.; Kispert, L. D. ENDOR Data Tabulations. In *Handbook of Electron Spin Resonance*; Poole, J. C. P., Farach, H. A., Eds.; AIP Press: Woodbury, NY, 1994; p 360.

(2) McConnell, H. M.; Heller, C.; Cole, T.; Fessenden, R. W. *J. Am. Chem. Soc.* **1960**, *82*, 766.

(3) McConnell, H. M.; Chesnut, D. B. *J. Chem. Phys.* **1958**, *28*, 107.

(4) McConnell, H. M.; Strathdee, J. *Mol. Phys.* **1959**, *2*, 129.

(5) Miyagawa, I.; Gordy, W. *J. Chem. Phys.* **1960**, *32*, 255.

(6) McCalley, R. C.; Kwiram, A. L. *J. Phys. Chem.* **1993**, *97*, 2888.

(7) Trammell, G. T.; Zeldes, H.; Livingston, R. *Phys. Rev.* **1958**, *110*, 630.

(8) Atherton, N. M. *Principles of Electron Spin Resonance*; Ellis Horwood PTR Prentice Hall: London, 1993.

(9) EPR software database, http://priscilla.niehs.nih.gov:591/ESR_Software/.

(10) Maruani, J. *J. Magn. Reson.* **1972**, *7*, 207.

(11) Maruani, J.; Roncin, J. *Chem. Phys. Lett.* **1973**, *23*, 449.

(12) Schlick, S.; Kevan, L. *J. Magn. Reson.* **1976**, *21*, 129.

(13) Sagstuen, E.; Hole, E. O.; Haugedal, S. R.; Lund, A.; Eid, O. I.; Erickson, R. *Nukleonika* **1997**, *42*, 353.

(14) Nam, J. W.; Regulla, D. F. *Appl. Radiat. Isot.* **1989**, *40*, 953.

(15) Goedkoop, J. A.; MacGillavry, C. H. *Acta Crystallogr.* **1957**, *10*, 125.

(16) Nelson, W. H. *J. Magn. Reson.* **1980**, *38*, 71.

(17) Sørnes, A. R.; Sagstuen, E.; Lund, A. *J. Phys. Chem.* **1995**, *99*, 16867.

(18) Busing, W. R.; Martin, K. O.; Levy, H. A. Report ORNL-TM-306; Oak Ridge National Laboratories: Oak Ridge, TN, 1964.

(19) Frisch, M. J.; Trucks, G. W.; Schlegel, H. B.; Scuseria, G. E.; Robb, M. A.; Cheeseman, J. R.; Zakrewski, V. G.; Montgomery, J. A., Jr.; Stratmann, R. E.; Burant, J. C.; Dapprich, S.; Millam, J. M.; Daniels, A. D.; Kudin, K. N.; Strain, M. C.; Farkas, O.; Tomasi, J.; Barone, V.; Cossi, M.; Cammi, R.; Mennucci, B.; Pomelli, C.; Adamo, C.; Clifford, S.; Ochterski, J.; Petersson, G. A.; Ayala, P. Y.; Cui, Q.; Morokuma, K.; Malick, D. K.; Rabuck, A. D.; Raghavachari, K.; Foresman, J. B.; Cioslowski, J.; Ortiz, J. V.; Stefanov, B. B.; Liu, G.; Liashenko, A.; Piskorz, P.; Komaromi, I.; Gomperts, R.; Martin, R. L.; Fox, D. J.; Keith, T.; Al-Laham, M. A.; Peng, C. Y.; Nanayakkara, A.; Gonzalez, C.; Challacombe, M.; Gill, P. M. W.; Johnson, B. G.; Chen, W.; Wong, M. W.; Andres, J. L.; Head-Gordon, M.; Replogle, E. S.; Pople, J. A. *Gaussian 98*, revision A.4; Gaussian, Inc.: Pittsburgh, PA, 1998.

(20) Portis, A. M. *Phys. Rev.* **1953**, *91*, 1071.

(21) Castner, J. T. G. *Phys. Rev.* **1959**, *115*, 1506.

(22) Lund, A.; Thuomas, K.-Å.; Maruani, J. *J. Magn. Reson.* **1978**, *30*, 505.

(23) Thuomas, K.-Å.; Lund, A. *J. Magn. Reson.* **1976**, *22*, 315.

(24) Lund, A.; Erickson, R. *Acta Chem. Scand.* **1998**, *52*, 261.

(25) Lefebvre, R.; Maruani, J. *J. Chem. Phys.* **1965**, *42*, 1480.

(26) Bergene, R.; Melø, T. B. *Biophysik* **1972**, *9*, 1.

(27) Sanderud, A.; Sagstuen, E.; Itagaki, Y.; Lund, A. *J. Phys. Chem. A* **2000**, *104*, 6372.

(28) Schlick, S.; Kevan, L. *J. Magn. Reson.* **1976**, *22*, 171.

(29) Höfer, P. Electron and Nuclear Spin Relaxation Effects in Pulsed ENDOR Spectroscopy. Presented at the 32nd Rocky Mountain Conference, Denver, Co. 1994.

(30) Oloff, H.; Hüttermann, J. *J. Magn. Reson.* **1980**, *40*, 415.

(31) Kikuchi, M.; Leray, N.; Roncin, J.; Joukoff, B. *J. Chem. Phys.* **1976**, *12*, 169.